Modeling Spiral Density Waves in Black Hole Accretion Disks

Joshua D. Gottlieb

under the direction of
Professor Edmund Bertschinger
Massachusetts Institute of Technology

Research Science Institute
30 July 2002

Abstract

When black holes or neutron stars are formed in close binary star systems, X-ray-emitting accretion disks are often created. Previous research has shown that the light output from these X-ray binaries flicker rapidly, a phenomenon called quasi-periodic oscillations (QPOs). The QPOs indicate that the accretion disks are not axisymmetric. In this paper, we undertake a theoretical investigation of one possible explanation for the lack of axisymmetry: spiral density waves. Using both analytical methods and computer simulations, we investigate accretion disk density under the spiral density wave model. The analyses indicate that spiral density waves in accretion disks can persist throughout time and are therefore a plausible explanation for the QPOs.

1 Introduction

Accretion disks around black holes or neutron stars are powerful kiloelectronvolt-range X-ray sources (Shapiro & Teukolsky 1983). In fact, accretion disk X-ray emission is commonly used to detect the existence of the compact objects (COs, includes black holes and neutron stars) themselves.

When a CO is formed very close to its companion star (the active star) in a binary system, it has a strong gravitational influence on particles near the edge of the active star. When this influence becomes greater than the active star's gravitational attraction, the particles approach the CO. Because they have angular momenta (and because angular momentum is conserved), they cannot fall directly to the event horizon or the star; instead, they enter into orbit. The orbiting material is collectively called the accretion disk.

Previous research (van der Klis 2000, Remillard et al 2002, using data from the Rossi X-ray Timing Explorer) has shown that the amount of X-ray light emitted from some CO accretion disks fluctuates with time in a quasi-periodic manner. These quasi-periodic oscillations (QPOs) indicate that the disks are not axisymmetric, or uniform: were they axisymmetric, there would be no method of varying the light intensity.

One possible form for the non-axisymmetries is *spiral density waves*. That is, accretion disks with QPOs could have regions of high density arranged in a classic spiral shape. These waves are analogous to regions of high star density forming spiral arms in spiral galaxies (Struck-Marcell 1990). We can therefore say that accretion disk density increases when near-parallel streams of gas approach each other.

Taking this idea to the extreme, we must consider the case when gas streams intersect. Because the streams are densely composed of particles, their intersection would result in a high frequency of particle collisions. In reality, however, particle collisions occur infrequently in accretion disks. In order for collisions to be common, the random kinetic velocities would have to be comparable to the orbital velocities, but observations that $T \approx 10^7$ K (Shaprio

& Tukolsky) rule out that possibility. In terms of the density model, gas stream intersection would cause the density to instantly jump instead of increasing smoothly. In singularity theory, a discontinuity in the density is called a caustic (Arnol'd 1992). Therefore, an important test for any density wave model is that it must be caustic-free, even as it evolves over time.

In this paper, we discuss the construction of accretion disk models with spiral density waves. We first create models analytically, and then by computer simulation. The computer models, generated by looking at the positions and orbits of many millions of particles, enable us to use the criterion above in order to consider the plausibility of density waves in real accretion disks.

We begin the discussion with a general consideration of orbital mechanics and perturbation theory (§§2.1 and 2.2), tools which we then apply to the relativistic situation around a black hole in §2.3. Finally, we will discuss the three main steps in our investigation: creating an axisymmetric disk by random sampling (§3), deforming the disk to a non-axisymmetric shape by displacing particles (§4), and evolving the disk over time (§5). The results of this investigation will determine whether or not the spiral density wave theory is plausible.

2 Orbital mechanics with perturbation theory

In order to model accretion disks we first must investigate orbital dynamics in a central potential. We expand the orbits using first-order perturbation theory in order to simplify calculations. Perturbation theory assumes that orbits are very close to circular. That is, if r is the distance from the gravitating object,

$$r(\tau) = r_0 - \epsilon(\tau) \quad \text{and} \quad \phi(\tau) = \phi_0 + \Omega_\phi \tau \tag{1}$$

where r_0 is the circular approximation of r and $\epsilon(\tau)$ is the correction. We use the symbol τ for the proper time measured by the particle. In the non-relativistic case, τ is equivalent to the universal Newtonian time t. We discuss the relativistic case in §2.3 below.

In this section, we first derive an exact solution for the orbital energy equation in any arbitrary central potential and then discuss the orbit with perturbation theory. We then evaluate the relativistic potential, which we need to use around black holes for a number of reasons. These are discussed more thoroughly in §5.

2.1 General orbits in a central potential

We can derive our orbital equations from two assumptions (Landau & Lifschitz 1993). The first one is the expression for angular momentum per unit mass.

$$\vec{\boldsymbol{L}} \equiv \vec{\boldsymbol{r}} \times \vec{\boldsymbol{v}} \tag{2}$$

where $\vec{\boldsymbol{v}} \equiv d\vec{\boldsymbol{r}}/d\tau$. For orbits in a central potential, angular momentum is conserved, or $d\vec{\boldsymbol{L}}/d\tau = \vec{\boldsymbol{0}}$ (Kleppner & Kolenkow 1973 §6.3). Then, by splitting $\vec{\boldsymbol{v}}$ into radial and tangential velocity components ($\vec{\boldsymbol{v}}_r$ and $\vec{\boldsymbol{v}}_t = r d\phi/d\tau$), and defining $\vec{\boldsymbol{e}}$ as the unit vector in any given direction, we have

$$L \equiv |\vec{\boldsymbol{L}}| = |\vec{\boldsymbol{r}} \times (v_r \vec{\boldsymbol{e}}_r + v_t \vec{\boldsymbol{e}}_r)| = r^2 \frac{d\phi}{d\tau}, \tag{3}$$

after using the fact that $|\vec{\boldsymbol{r}} \times \vec{\boldsymbol{e}}_r| = 0$.

Our next assumption pertains to the orbital energy. We assume that orbits in a central potential $V(r)$ have energy per unit mass

$$E \equiv \frac{1}{2}\vec{\boldsymbol{v}}^2 + V(r) = \frac{1}{2}\left(v_r \vec{\boldsymbol{e}}_r + v_t \vec{\boldsymbol{e}}_t\right)^2 + V(r) = \frac{v_r^2}{2} + \frac{r^2 v_t^2}{2} + V(r) = \frac{1}{2}\left(\frac{dr}{d\tau}\right)^2 + \frac{L^2}{2r^2} + V(r), \tag{4}$$

since we know that $\vec{\boldsymbol{e}}_r \perp \vec{\boldsymbol{e}}_t \Rightarrow \vec{\boldsymbol{e}}_r \cdot \vec{\boldsymbol{e}}_t = 0$. We now define the effective potential $V_{\text{eff}}(r)$ as

$$V_{\text{eff}}(r) \equiv V(r) + \frac{L^2}{2r^2}. \tag{5}$$

Solving equation (4) for $dr/d\tau$ and using the expression for $V(r)$ from equation (5), we have an expression for radial velocity:

$$\frac{dr}{d\tau} = [2E - 2V_{\text{eff}}(r)]^{1/2}. \tag{6}$$

2.2 Nearly Circular Orbits

In order to approximate an orbit with perturbation theory, we must calculate equations of motion $dr/d\tau$ and $d\phi/d\tau$ for any arbitrary $V_{\text{eff}}(r)$, and then integrate them.

Substituting $r = r_0 - \epsilon(\tau)$ into equation (18) and Taylor expanding $V_{\text{eff}}(r)$ about $r = r_0$, we get

$$\left(\frac{d\epsilon}{d\tau}\right)^2 + \Omega_r^2 \epsilon^2 = 2E - 2V_{\text{eff}}(r), \tag{7}$$

where

$$\Omega_r \equiv \left(\frac{d^2 V_{\text{eff}}}{dr^2}\right)^{1/2}\Bigg|_{r=r_0}. \tag{8}$$

The solution of equation (7) gives

$$r(\tau) = r_0 - \epsilon_0 \cos[\Omega_r \tau + \theta_0] = r_0 - \frac{(2E - 2V_{\text{eff}})^{1/2}}{\Omega_r} \cos(\Omega_r \tau + \theta_0). \tag{9}$$

Note that the appearance of Ω_r as the frequency constant within the cosine argument proves that it is the orbital frequency in radius; the frequency of cycling between the minimal and maximal radii. This does not necessarily equal Ω_ϕ, the angular frequency in equation

(1). In order to determine Ω_ϕ, we differentiate equation (1) with respect to τ and then use our expression for $d\phi/d\tau$ from equation (3). After replacing $r = r_0$ for the circular approximation of Ω_ϕ, we have

$$\Omega_\phi = \frac{L}{r_0^2} \Rightarrow \phi(\tau) = \phi_0 + \Omega_r \tau \tag{10}$$

and thus our second equation of motion.

2.3 Solution for the relativistic central potential

In order to evaluate orbits with the Schwarzschild metric (relativity around a non-rotating black hole), we need to determine $r(t)$ and $\phi(t)$. This requires two assumptions about relativity. We must start with the Schwarzschild central potential, as well as the relationship between proper time and *universal time*.

We begin by considering the central potential for a Schwarzschild black hole. It is given by Ohanian & Ruffini (1994 §7.6) as

$$V_{\text{eff}}(r) = -\frac{GM}{r} + \frac{L^2}{2r^2}(1 - 2x), \quad x \; equiv \frac{GM}{rc^2} \tag{11}$$

equivalent to the Newtonian potential with an extra term of order r^{-3}. By setting $dV_{\text{eff}}/dr = 0$ at $r = r_0$, we find

$$r_0 = \frac{L^2 \pm (L^4 - 12G^2M^2L^2c^{-2})^{1/2}}{2GM}. \tag{12}$$

This result implies

$$L^2 = \frac{GMr_0^2}{3GM/c^2 - r_0} = \frac{GMr_0}{1 - 3x}. \tag{13}$$

In relativistic situations, time is observer-dependent. We must therefore distinguish

between *universal time*, t, (time according to an observer at rest with respect to the central object and at effectively infinite distance from our system) and local proper time τ, as observed in the particles' rest frames. According to Ohanian & Ruffini (1994 §8.1), t and τ are related by

$$c^2 d\tau^2 = c^2(1-2x)dt^2 - (1-2x)^{-1}dr^2 - r^2 d\phi^2, \tag{14}$$

with the speed of light c no longer being set equal to unity, as done in Ohanian & Ruffini. This expression accounts for gravitational redshift as well as the special relativistic Doppler shift. We now reduce this equation to a circular approximation, in which $dr/d\tau = 0$ and $d\phi/d\tau$ is given by equation (3). Then we use the expression for L^2 in equation (13), followed by the definition of x in equation (11) and then division by $d\tau^2$, to find

$$\frac{dt}{d\tau} = \left(\frac{1 + L^2 r_0^{-2} c^{-2}}{1-2x}\right)^{1/2} = (1-2x)^{-1/2}\left(\frac{1-2x}{1-3x}\right)^{1/2} = (1-3x)^{-1/2}. \tag{15}$$

Because $1-3x$ is independent of t and τ, integration tells us that

$$\frac{t}{\tau} = \frac{dt}{d\tau}. \tag{16}$$

In order to complete our relativistic perturbation equations we must consider the radial and angular frequencies. These change when we move into the relativistic case because $t \neq \tau$. We call the new frequencies ω_r and ω_ϕ, respectively.

According to equation (16), replacing τ in equations (9) with t will only demand an additional factor of $d\tau/dt$. Because this ratio is constant for a given orbit (in our circular approximation), we absorb it into the frequency. Therefore r depends only on t. This means

that

$$\omega_r = \frac{d\tau}{dt}\left(\frac{d^2V_{\text{eff}}}{dr^2}\right)^{1/2}_{r=r_0} \quad \text{and} \quad \omega_\phi = \frac{L}{r_0^2}\frac{d\tau}{dt}. \tag{17}$$

Calculating ω_r is now straightforward. We differentiate $V_{\text{eff}}(r)$ with respect to r twice, and then evaluate it at $r = r_0$ to obtain

$$\omega_r^2 = \left(\frac{d\tau}{dt}\right)^2 \left.\frac{d^2V_{\text{eff}}}{dr^2}\right|_{r=r_0} = (1-3x)\left(-\frac{2GM}{r_0^3} + \frac{3L^2}{r_0^4} - \frac{12GML^2}{c^2r_0^5}\right) = \frac{GM}{r_0^3}(1-6x) \tag{18}$$

after using equations (13) and (11).

We can similarly calculate ω_ϕ:

$$\omega_\phi = \frac{L}{r_0^2}\frac{d\tau}{dt} = \left[\frac{GMr_0}{(1-3x)r_0^4}\right](1-3x)^{1/2} = \frac{(GM)^{1/2}}{r_0^{3/2}(1-3x)^{1/2}}(1-3x)^{1/2} = \left(\frac{GM}{r_0^3}\right)^{1/2}. \tag{19}$$

Our equations of relativistic orbits in perturbation theory are now

$$r(\tau) = r_0 - \epsilon_0\cos(\omega_r t + \theta_0), \quad \phi(\tau) = \phi_0 + \omega_\phi\tau. \tag{20}$$

If we set the determinant of equation (12) equal to zero, we can solve for the innermost stable circular orbit. Then,

$$r_{0,\min} = \frac{L^2}{2GM} = \frac{6GM}{c^2} = 3r_S, \tag{21}$$

where $r_S = 2GMc^{-2}$ is the Schwarzschild radius for a black hole of mass M (Ohanian & Ruffini, §8.1). This is confirmed using the expression for ω_r in equation (18): at $r = r_{0,\min}$,

$$\omega_r = \left(\frac{GM}{r_0^3}\right)^{1/2}(1-6x)^{1/2} = \left(\frac{GM}{r_0^3}\right)^{1/2}\left(1 - \frac{6GMc^{-2}}{6GMc^{-2}}\right)^{1/2} = 0. \tag{22}$$

A frequency of zero is allowed; it means that the radius never changes and we have, as expected, the innermost stable circular orbit. At $r < r_{0,\min}$, however, $1 - 6x < 0$ and its square root is not a real number. Because every orbit must have a real frequency no orbit can exist at $r < r_{0,\min}$.

3 Axisymmetric disk models

Now that we have evaluated the relativistic orbits we can begin to model accretion disks. The first of our three steps in accretion disk modeling is to place many particles at random in a plane so as to produce any desired density profile in the disk. We generate random positions for each particle using polar coordinates $(\bar{r}, \bar{\phi})$.

In this section, we look only at axisymmetric disks. Because of that, the density profile n_0 (where the subscript zero denotes the circular disk) depends only on $\bar{r}$; we can measure the density along any radial line we choose. In order to make the disk axisymmetric, we distribute $\bar{\phi}$ uniformly on $[0, 2\pi)$; that is, every value on the interval $[0, 2\pi)$ has an equal probability of being selected. The radius $\bar{r}$ is based on a uniform $[0, 1]$ distribution that has been modified to give the desired $n_0(\bar{r})$. Thus, the goal of this section is to derive an algorithm for modifying the uniform distribution to obtain any $n_0(\bar{r})$.

In order to derive this algorithm, we must calculate dN, the small number of particles in some small area $d\bar{A}$, two different ways:

$$dN = n_0(\bar{r})d\bar{A} = n_0(\bar{r})\bar{r}d\bar{r}d\bar{\phi}, \quad dN = \frac{d\xi d\bar{\phi}}{2\pi}N_{\text{tot}}. \tag{23}$$

The first method uses the number density n_0 of number of particles per area, multiplied by the area $d\bar{A}$. For a sector of an annulus, $d\bar{A}$ is calculated by approximating it as a rectangle with width $\bar{r}d\bar{\phi}$ and radial length $d\bar{r}$.

The second expression for dN depends on the uniform distribution. Let us define ξ as

the random variable uniform in $[0, 1]$. Then $d\xi$ is the probability that a given particle is in some radial space $d\bar{r}$. We multiply this by the angular probability, which is equal to $d\bar{\phi}/2\pi$ because of the uniformity in angular distribution. This gives the probability that a given particle is in $d\bar{A}$, or, equivalently, the fraction of all particles that are in $d\bar{A}$. In order to get dN, the finite number of particles in $d\bar{A}$, we multiply by the total number of particles.

Combining the two parts of equations (23), we have

$$n_0(\bar{r}) = \frac{dN}{d\bar{A}} = \frac{d\xi d\bar{\phi}}{d\bar{A}} \frac{N_{\rm tot}}{2\pi}. \tag{24}$$

In order to use this expression, we must calculate $d\xi$. Consider the function $f(\xi)$, which we require to be monotonic (so that we can take its inverse below) with $f(0) = 0$ and $f(1) = 1$. This function allows us to sample $\bar{r}$ using

$$\bar{r}(\xi) = \bar{r}_{\rm min} + (\bar{r}_{\rm max} - \bar{r}_{\rm min}) f(\xi), \tag{25}$$

where $\bar{r}_{\rm min}$ and $\bar{r}_{\rm max}$ are the inner and outer edges of the disk, respectively. We subtract $\bar{r}_{\rm min}$, divide by $(\bar{r}_{\rm max} - \bar{r}_{\rm min})$ and take the inverse of each side, giving

$$\xi = f^{-1}\left(\frac{\bar{r} - \bar{r}_{\rm min}}{\bar{r}_{\rm max} - \bar{r}_{\rm min}}\right). \tag{26}$$

We define $y \equiv (r - \bar{r}_{\rm min})/(\bar{r}_{\rm max} - \bar{r}_{\rm min})$, noting that $dy = dr/(\bar{r}_{\rm max} - \bar{r}_{\rm min})$, for purposes of simplicity. Differentiating equation (26) with respect to ξ and multiplying by $d\xi$ yields

$$d\xi = df^{-1}(y). \tag{27}$$

If we use this in equation (24), solve for df^{-1}, and integrate, we have

$$f^{-1}\left(\frac{\bar{r} - \bar{r}_{\rm min}}{\bar{r}_{\rm max} - \bar{r}_{\rm min}}\right) = \int_{\bar{r}_{\rm min}}^{\bar{r}} \frac{2\pi \bar{r}' n_0(\bar{r}')}{N_{\rm tot}} d\bar{r}', \tag{28}$$

where $\bar{r}'$ is a dummy variable of integration. We can then take the inverse of f^{-1} to get $f(\xi)$, which allows us to create an axisymmetric accretion disk.

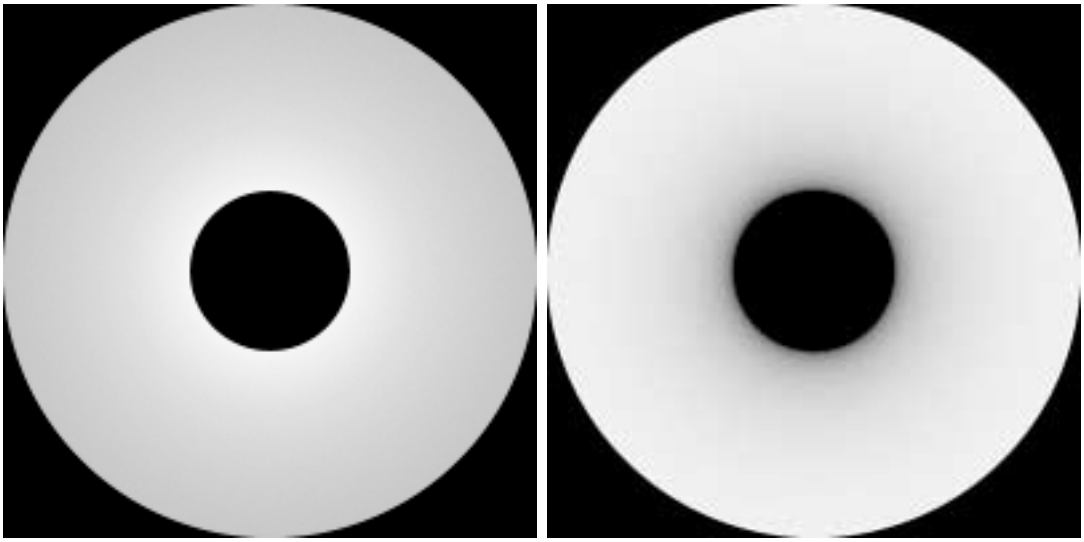

Figure 1: Two axisymmetric density models in Keplerian disks, generated from equation (25): the first was generated with $f(\xi) = \xi$ and the second with $f(\xi) = \xi^{1/2}$. The density of the first one decreases outwards and the density of the second increases with r.

4 Perturbed disk models

We now allow our accretion disks to be non-axisymmetric by replacing the coordinates in §3, $(\bar{r}, \bar{\phi})$, with new coordinates (r, ϕ). We determine (r, ϕ) by using mapping functions of $(\bar{r}, \bar{\phi})$, which are generated just as in §3. These mapping functions, F and G, can be expressed as

$$r = F(\bar{r}, \bar{\phi}) = \bar{r} - \epsilon_0(\bar{r}, \bar{\phi}), \quad \phi = G(\bar{r}, \bar{\phi}) = \bar{\phi} + \phi_0(\bar{r}, \bar{\phi}). \tag{29}$$

The perturbation functions are required to be periodic, such that $\epsilon_0(\bar{r}, \bar{\phi} + 2\pi) = \epsilon_0(\bar{r}, \bar{\phi})$ and $\phi_0(\bar{r}, \bar{\phi} + 2\pi) = \phi_0(\bar{r}, \bar{\phi})$ (that is, the period must be an integer unit fraction of 2π) so that all particles lying at a given original point $(\bar{r}, \bar{\phi} + 2\pi n)$ are mapped to the same (r, ϕ). They must be smooth and once-differentiable with respect to both $\bar{r}$ and $\bar{\phi}$. Additionally,

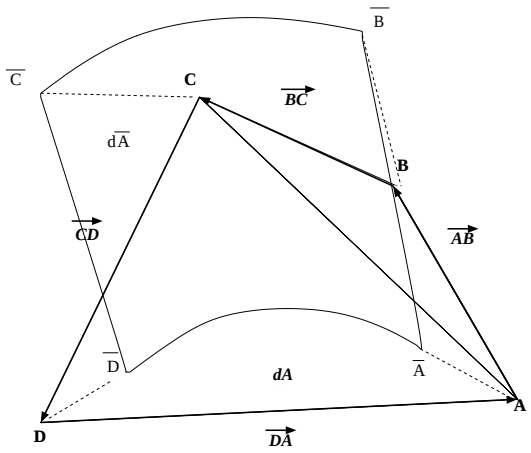

Figure 2: A mapping of $(\bar{r}, \bar{\phi}) \to (r, \phi)$ in order to calculate the area of area element dA.

recall our fundamental assumption about perturbations: $\epsilon_0^2 \ll r_0^2$. The final density function can be calculated using one invariant: the number of objects in our region. Although the region is deformed by the mapping, the particles are required to stay within it. As in §3, we calculate the density by equating the number of particles in a small area two different ways:

$$dN = n_0(\bar{r})d\bar{A}, \quad dN = n(r, \phi)dA. \tag{30}$$

Here $d\bar{A}$ is the area of a small region before the mapping and dA is the area after hte mapping. Thus

$$n(r, \phi) = n_0(\bar{r})\frac{d\bar{A}}{dA}. \tag{31}$$

Because n depends on the new area dA, we must now calculate dA, which may be more complex than $d\bar{A}$.

Figure 2 illustrates the mapping of an area $d\bar{A}$, where the corner points are defined as $\bar{A} = (\bar{r}, \bar{\phi})$, $\bar{B} = (\bar{r} + d\bar{r}, \bar{\phi})$, $\bar{C} = (\bar{r} + d\bar{r}, \bar{\phi} + d\bar{\phi})$, and $\bar{D} = (\bar{r}, \bar{\phi} + d\bar{\phi}, \bar{r} + d\bar{r}, \bar{\phi})$. Then, each of these points is mapped using F and G to its respective new coordinate. The new area dA can be approximated by a quadrilateral, $ABCD$, which can be split into two

triangles, ABC and CDA. The areas of each of the triangles can be calculated as one-half the magnitude of the vector product of the two sides labeled as vectors. Then our vectors representing sides of quadrilaterals can be expressed in terms of F and G. For example, $\overrightarrow{AB} = (dr, rd\phi) = \left(\frac{\partial F}{\partial \bar{r}} d\bar{r}, r\frac{\partial G}{\partial \bar{r}} d\bar{r}\right)$. This gives, for our final area,

$$dA = \left|\overrightarrow{AB} \times \overrightarrow{BC} + \overrightarrow{CD} \times \overrightarrow{DA}\right| = r d\bar{r} d\bar{\phi} \left|\frac{\partial F}{\partial \bar{r}}\frac{\partial G}{\partial \bar{\phi}} - \frac{\partial F}{\partial \bar{\phi}}\frac{\partial G}{\partial \bar{r}}\right| = r d\bar{r} d\bar{\phi} J, \tag{32}$$

where $J \equiv ||\partial(F, G)/\partial(\bar{r}, \bar{\phi})||$ is the Jacobian determinant. Note that we sum the vector products before taking the magnitude because it is possible for one of the areas to be negative. If we have a concave quadrilateral, one of the triangles would include an area exterior to the quadrilateral, which would be subtracted.

The expression for dA can be replaced into equation (31) to obtain

$$n(r, \phi) = \sum_{\bar{r}(r), \bar{\phi}(r)} n_0(\bar{r}) \frac{\bar{r}}{r} J^{-1} = \sum_{\bar{r}(r), \bar{\phi}(r)} n_0(\bar{r}) \frac{\bar{r}}{r} \left|\frac{\partial F}{\partial \bar{r}}\frac{\partial G}{\partial \bar{\phi}} - \frac{\partial F}{\partial \bar{\phi}}\frac{\partial G}{\partial \bar{r}}\right|^{-1}. \tag{33}$$

The expression is summed over all values $\bar{r}$ that get mapped to the given r, as there could be more than one.

If we reduce this formula to the case when $\phi = \bar{\phi}$ and F depends only on $\bar{r}$, we discover that $\partial G/\partial \bar{r} = 0$, $\partial G/\partial \bar{\phi} = 1$, and $\partial F/\partial \bar{r} = dr/d\bar{r}$. Thus, the density becomes

$$n(r, \phi) = \sum_{\bar{r}(r), \bar{\phi}(r)} n_0(\bar{r}) \frac{\bar{r}}{r} \left|\frac{\partial F}{\partial \bar{r}}\right|^{-1} = \sum_{\bar{r}(r), \bar{\phi}(r)} n_0(\bar{r}) \frac{\bar{r}}{r} \left|\frac{dr}{d\bar{r}}\right|^{-1}. \tag{34}$$

The density is proportional to the inverse derivative of $r(\bar{r})$. So as $r(\bar{r})$ flattens out and its derivative decreases, the density increases. Any point where the derivative is zero has an infinite discontinuity in the density, or a caustic.

Figure 3 demonstrates caustics of this type. This simulated disk has density $n_0(\bar{r}) \propto \bar{r}^{-1}$,

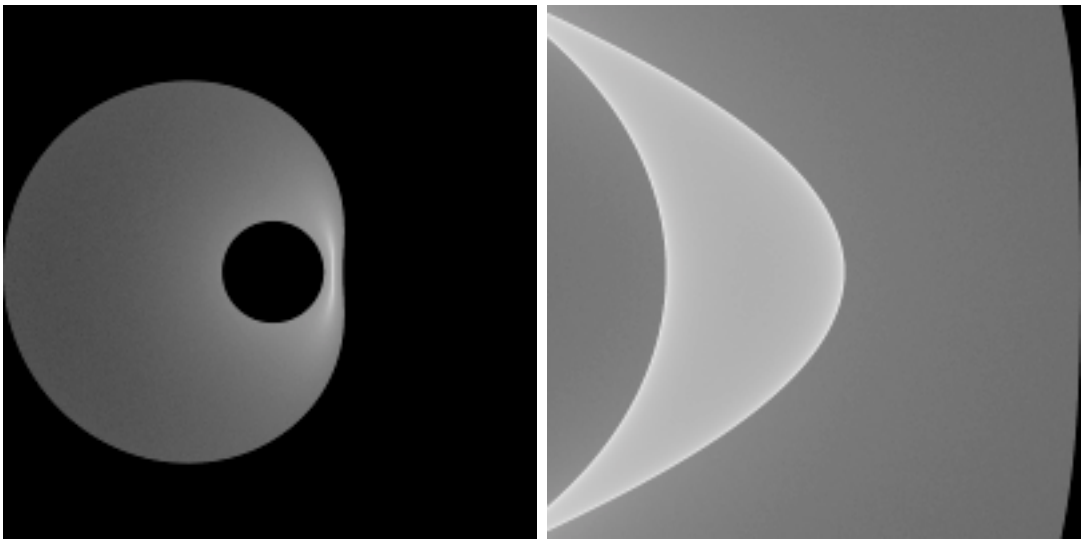

Figure 3: A caustic in an accretion disk, generated with the cubic function (35). The right-hand side of the first frame is expanded in the second frame to give a (vertically stretched) higher-resolution view of the two caustics and the high-density area between them.

or $f(\xi) = \xi$. The perturbation function is

$$\epsilon_0(\bar{r}, \bar{\phi}) = (a\bar{r}^3 + b\bar{r}^2 + c\bar{r} + d)\cos(\bar{\phi}), \tag{35}$$

where $a = -3.84615 \cdot 10^{-15}$, $b = 1.49254 \cdot 10^{-7}$, $c = -0.9$, and $d = -5 \cdot 10^5$. The density on the right-hand side of the disk peaks at the bright lines (which are magnified the second frame), and is much higher between them than outside of them. We tested this disk by analyzing the density along the line $\phi = \bar{\phi} = 0$ based on the simulated data as well as our analytical model. The results were in agreement.

5 Time evolution in disk models

Although we can now manipulate static disks by varying F, G, and thus the density n, we are interested in time variability. For each particle, we map the original position $(\bar{r}, \bar{\phi})$ onto (r, ϕ) and then allow time evolution.

The mapping functions F and G from equations (29) can be modified to incorporate time when taken together with equations (20). We simply allow ϵ_0, θ_0, and ϕ_0 to be functions of $\bar{r}$ and $\bar{\phi}$. The result is that

$$r(t) = \bar{r} - \epsilon_0(\bar{r}, \bar{\phi}) \cos[\omega_r(\bar{r})t + \theta_0(\bar{r}, \bar{\phi})] \quad \text{and} \quad \phi(t) = \bar{\phi} + \phi_0(\bar{r}, \bar{\phi}) + \omega_\phi(\bar{r})t. \tag{36}$$

The functions ϵ_0, θ_0, and ϕ_0 are required to be periodic in $\bar{\phi}$ (and θ_0 specifically must have a period of 2π) so that the mapping is identical for all particles at a given position, despite the use of polar coordinates.

As before, we look at the accretion disk density by considering the Jacobian determinant J. As J decreases, we get a density wave; furthermore, as $J \to 0$, we get a caustic.

In order to ensure $J \neq 0$ for all (r, ϕ, t), we must require the Jacobian not to change sign. For any given $(\bar{r}, \bar{\phi})$, the only variable is t. The Jacobian has terms sinusoidal in t which would naturally change sign every π/ω_r. As t becomes large, the terms linear in t (grouped together on the second line) would naturally dominate and cause the sign changes. We must therefore be able to set them equal to zero and allow the terms on the first line to prevent the sign change. Because $\mu(\bar{r})$ is predetermined, the coefficient of the cosine is equal to zero only when $\partial\epsilon_0/\partial\bar{\phi} = 0$, implying that ϵ_0 is only a function of $\bar{r}$. Looking at the sine term, we need to ensure

$$1 + \frac{\partial\phi_0}{\partial\bar{\phi}} - \mu\frac{\partial\theta_0}{\partial\bar{\phi}} = 0, \quad \mu \equiv \frac{d\omega_\phi}{d\omega_r}. \tag{37}$$

Integrating this with respect to ϕ and solving for ϕ_0,

$$\phi_0(\bar{r}, \bar{\phi}) = \mu(\bar{r})\theta_0(\bar{r}, \bar{\phi}) - \bar{\phi} + \eta(\bar{r}), \tag{38}$$

where $\eta(\bar{r})$ is the constant of integration. It can depend on $\bar{r}$ because $\bar{r}$ is independent of

the variable of integration, $\bar{\phi}$. If we replace this into equation (36), we find that

$$\phi(t) = \mu(\bar{r})\theta_0(\bar{r}, \bar{\phi}) + \eta(\bar{r}) + \omega_\phi(\bar{r})t. \tag{39}$$

This will allow us to generate caustic-free disks for any given functions $\theta_0(\bar{r}, \bar{\phi})$ and $\eta(\bar{r})$. However, the disks will have finite discontinuities (edges) if ϕ_0 and θ_0 are not both periodic with period 2π. This happens if $\mu \neq 1$.

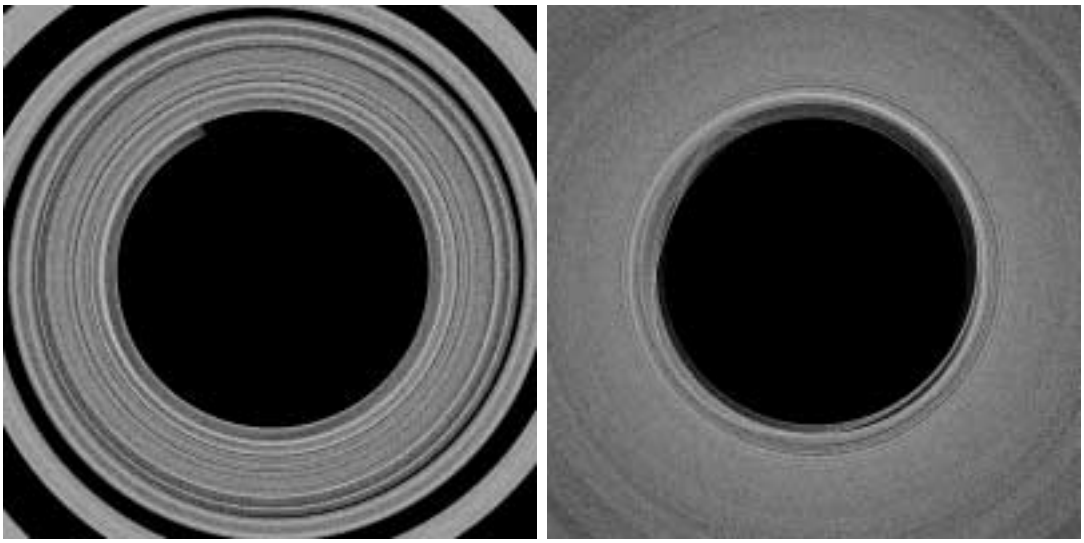

Figure 4: The accretion disk model on the left has initial conditions which approximate the necessary conditions for the elimination of caustics. The one on the right is far from those conditions. Both images were taken after 1000 orbits in the model.

Figure 4 shows two accretion disks modeled after 1000 orbits. The first one meets the criteria in equations (39) and the second does not. Although these disks are imperfect (as edges are visible in the first one), they demonstrate qualitatively the possibility for eliminating caustics by using more precise equations.

6 Conclusion

Our analytical work has shown that it is possible to create spiral density waves in first-order accretion disk models for the Schwarzschild black hole without forming caustics and thereby rendering the model unrealistic. By carefully defining initial parameters, we can create accretion disk models which appear to match emperically observed situations.

Although our computer simulation has not yet created an accretion disk that matches the paramters above, it has successfully modeled many aspects of accretion disks, including mapping, caustics, and time evolution. These individual aspects are critical to understanding accretion disks.

The logical progression from this work is to complete the realistic accretion disk model by truly avoiding caustics. This appears to be a promising area for future research and it would naturally lead to an even larger step. Once an accurate model has been completed it will be possible to compare its simulated light emission with emperical light curves and determine the validity of our model and whether our criteria were accurate and sufficient.

Acknowledgments

I am greatly indebted to Professor Edmund Bertschinger, my mentor throughout this work, for his continued support, assistance, and teaching. Without his suggestions for the project's basic premise, logical progression, numerous steps throughout, and final report, I would have been unable to begin to learn astrophysics. Professor Bertschinger has taught me how naturally original research and previous knowledge are intertwined.

Many thanks to Ben Rahn, Vivek Venkatachalam, Jacinta Conrad, and Molly Peeples for editing this paper and helping me to see and repair the flaws that must arise. Special thanks to Vivek for his advice throughout the duration of my research.

Finally, I would like to thank the Center for Excellence in Education (CEE) for facilitating this research by allowing me to attend the Research Science Institute (RSI) in 2002. Dr. John

Dell, Matt Cain, as well as my tutors, Kendrick Kay and Paul Dutka-Chirichetti, and the rest of the RSI staff, have assisted me throughout RSI and have made my experience complete and enjoyable. along with the rest of the staff, have made my experience complete and enjoyable. I am grateful to Dr. Dell for initiating my contact with Professor Bertschinger.

References

[1] Arnol'd, V.I., *Catastrophe Theory*, 3rd English Ed. (Berlin: Springer-Verlay, 1992)

[2] Goldstein, H, *Classical Mechanics* (Reading, Mass.: Addison-Wesley, 1965)

[3] Kleppner, D. & R.J. Kolenkow, *An Introduction to Mechanics* (New York: McGraw-Hill, 1973)

[4] Landau, L.D. & E.M. Lifschitz, *Course of Theoretical Physics: Volume 1, Mechanics*, 3rd Ed. (Oxford: Butterworth-Heinemann Ltd., 1993)

[5] Ohanian, H. & R. Ruffini, *Gravitation and Spacetime*, 2nd Ed. (New York: W.W. Norton & Co., 1994)

[6] Remillard, R.A., M.P. Muno, J.E. McClintock, J.A. Orosz, 2002, Ap.J. (in press); arXiv:astro-ph 0202305

[7] Shapiro, S.L. & S.A. Tukolsky, *Black Holes, White Dawrfs, and Neutron Stars: the Physics of Compact Objects* (New York: John Wiley & Sons)

[8] Struck-Marcell, C. 1990, Astron. J., 99, 71

[9] van der Klis, M. 2000, Annual Review of Astronomy and Astrophysics, 38, 717-760